Synthesis and characterization of a granular Fe–Ge layer by ion implantation and subsequent ion beam annealing

2007 J. Phys.: Condens. Matter 19 096003

(http://iopscience.iop.org/0953-8984/19/9/096003)

IOP PUBLISHING JOURNAL OF PHYSICS: CONDENSED MATTER

J. Phys.: Condens. Matter **19** (2007) 096003 (11pp) doi:10.1088/0953-8984/19/9/096003

Synthesis and characterization of a granular Fe–Ge layer by ion implantation and subsequent ion beam annealing

S Amirthapandian[1], B K Panigrahi[1], M Rajalakshmi[1], S Kalavathi[1], B Sundaravel[1], Ajay Gupta[2] and A Narayanasamy[3]

[1] Materials Science Division, Indira Gandhi Centre for Atomic Research, Kalpakkam-603 102, India
[2] UGC-DAE Consortium for Scientific Research, University Campus, Indore-452 017, India
[3] Materials Science Centre, Department of Nuclear Physics, University of Madras, Guindy Campus, Chennai-600 025, India

E-mail: pandian@igcar.gov.in

Received 31 July 2006, in final form 3 January 2007
Published 12 February 2007
Online at stacks.iop.org/JPhysCM/19/096003

Abstract

Ge[111] was implanted with Fe ions with an energy of 60 keV at various ion fluences. The structural properties were characterized by Raman scattering and grazing incidence x-ray diffraction (GIXRD) measurements. Raman scattering reveals the amorphization of Ge at a fluence of 5×10^{15} ions cm^{-2}. With further irradiation, a TO-like phonon mode evolves and the full-width at half-maximum (FWHM) of this mode increases with fluence. The amount of bond disorder was estimated from the FWHM of the TO-like phonon mode. The *a*-Ge is recrystallized by ion beam annealing of the sample at 250 °C with 1 MeV Ge^+ ions. The GIXRD measurements also support the amorphization and crystallization of Ge. The presence of Fe nanoclusters was observed in implanted samples by using low-frequency Raman scattering (LFRS). The formation of Fe nanoclusters is attributed to the irradiation process itself and thermal or radiation enhanced diffusivity is absent.

1. Introduction

Energetic ferromagnetic ions can be directly implanted into a non-magnetic matrix at a certain depth. Since the ferromagnetic ions are immiscible, these ions will precipitate as atomic clusters having nanometric dimensions. Ion beam synthesis of metal/semiconductor nanoclusters in various matrices like metals, semiconductors and insulators has attracted attention due to novel properties of the nanoclusters and their application in optical, magnetic and electronic industries. Using an ion beam one can synthesize the nanoclusters as well tailor their size and size distribution. Since ion implantation is a non-equilibrium process, it gives rise to new metastable phases with different properties. At low concentrations of Fe (<25 at.%), the

heat of mixing of the Fe–Ge system is positive, i.e. there is immiscibility [1]. When metallic particles are embedded in a semiconductor, the presence of the Schottky well changes the carrier concentration. If the band gap is lower, then the Schottky well is correspondingly lower, and as a result the depletion region around each metallic cluster is substantially reduced and the carrier concentration is enhanced. It should be noted that Ge has a small band gap with a high carrier mobility. Therefore, it is very easy to produce a large giant magnetoresistance (GMR) effect.

Ma *et al* [2, 3] grew ultra-thin Fe films on Ge[100] surfaces and found that no significant intermixing occurred for temperatures below 160 °C and that the FeGe alloy was formed only between 160 and 400 °C. Phase separation was observed in sequentially sputtered amorphous FeGe films [4]. Regan *et al* [4] observed that the Ge atoms are distributed homogeneously while the Fe atoms are distributed inhomogeneously in the sputtered FeGe films. The phase separation phenomenon observed in the amorphous FeGe system is considered to be essential for the preparation of granular materials where magnetic materials are immiscible in a non-magnetic metal matrix.

Granular materials can also be prepared by direct ion implantation. Venugopal *et al* have reported the magnetic properties of Fe ion-implanted Ge crystal [5]. These authors have observed negative magnetoresistance (8% of magnetoresistance at room temperature with a field of 0.8 T) for the Fe-implanted Ge samples and attributed it to the existence of magnetic clusters in the implanted layer. The same authors have also reported that low dose (2×10^{16} ions cm^{-2}) implantation causes the formation of Fe_3Ge precipitates whereas high dose (2×10^{17} ions cm^{-2}) implantation causes the formation of Fe precipitates [6]. However, in these experiments there was no independent control over the target temperature during implantation; for a dose of 2×10^{17} ions cm^{-2} the target temperature increases to 210 °C due to beam heating. The exact mechanism of the formation of Fe precipitates in Ge upon Fe ion implantation has not been understood. This motivated us to study the optical and structural properties of Fe-implanted Ge.

In the present paper, we report the optical and structural properties of Fe-implanted Ge in order to understand the mechanism of formation of Fe precipitates in a Ge matrix.

2. Experimental details

The c-Ge[111] wafer was implanted with 60 keV ^{56}Fe and ^{57}Fe ions of different fluences using a 200 kV isotope separator/ion implanter available at the Saha Institute of Nuclear Physics, Kolkata. The range of Fe ions is 345 Å with a straggling of 197 Å as found from SRIM 2003. The presence of the isotopes ^{56}Fe and ^{57}Fe as well as their concentration ratio was checked with secondary ion mass spectroscopy (SIMS) experiments. The range (330 Å) of Fe concentration matches with the range of 345 Å for 60 keV Fe ions in Ge. The GIXRD studies were performed using a STOE GmbH (Germany) x-ray diffractometer in parallel beam geometry. In order to get the diffraction from the implanted region, a glancing angle of 0.5° was chosen for the Cu-K_α radiation. The glancing angle of 0.5° is greater than the critical angle corresponding to total external reflection for Ge (0.3°). The x-ray probing depth was 5700 Å which is greater than the range (330 Å) of Fe^+ ions. For investigation of the local environment of implanted Fe atoms, the conversion electron Mössbauer spectroscopy (CEMS) measurements were performed with a ^{57}Co (Rh) radioactive source of strength ∼25 mCi. The conversion electrons were detected by a He/CH_4 (5% methane) gas flow proportional counter. The velocity calibration was done with a natural iron absorber. The spectral profiles were analysed by means of the NORMOS code developed by Brand [7]. The isomer shifts are given relative to natural iron at room temperature. The magnitude of the magnetic hyperfine

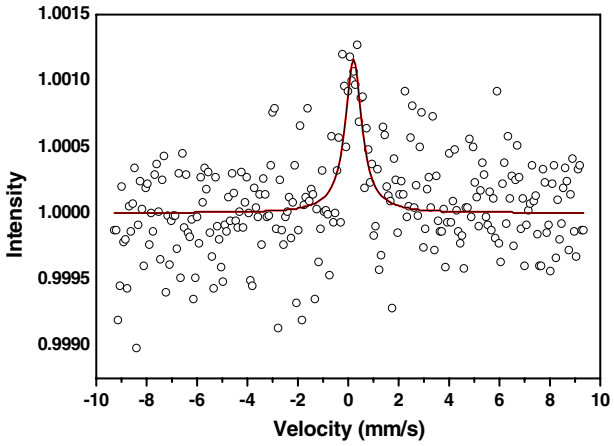

Figure 1. The conversion electron Mössbauer spectrum of the 60 keV Fe^+ ion-implanted Ge[111] to a fluence of 2×10^{17} ions cm^{-2}.

fields at Fe sites is assumed to be approximately proportional to the Fe magnetic moments. For further structural information, the Raman scattering measurements on the unimplanted and the Fe^+ ion-implanted samples were carried out in backscattering geometry. The samples were excited with a 488 nm argon ion laser beam of 200 mW power focused to a spot size of 25 μm on the sample. The backscattered light from the sample was collected using a camera lens and focusing lens, dispersed by a double grating monochromator (SPEX model 14018) and detected using a thermoelectrically cooled photomultiplier tube (ITT–FW 130) operated in photon counting mode. A microprocessor based data acquisition/automation system was used to record spectra at room temperature. The atomic force microscopy (AFM) measurements were carried out using a Solver PRO scanning probe microscope (NT-MDT, Russia). The tapping mode was used to study the surface modification on the Fe^+ ion-implanted Ge.

3. Results and discussion

Figure 1 shows the conversion electron Mössbauer spectrum of the sample implanted with 60 keV Fe^+ ions with a fluence of 2×10^{17} ions cm^{-2}. The spectrum shows a broad singlet with an isomer shift of 0.20 mm s^{-1}. Earlier Mössbauer studies on ion beam mixed Fe–Ge bilayers show a sextet with a hyperfine field of 11.5 T attributed to the crystalline hexagonal FeGe phase [8]. Further, post-annealing of the ion beam mixed sample at 625 °C showed the nucleation and growth of magnetic phases with hyperfine fields such as Fe_3Ge (21.8 T, 24.0 T) and Fe_5Ge_3 (13.6, 21.4, 25.6 T) [8]. The absence of such a sextet in the present experiment shows that the FeGe phases Fe_3Ge and Fe_5Ge_3 are not formed. The amorphous FeGe alloy used to show a doublet [9] and the absence of such a doublet in the present experiment rules out the formation of the a-FeGe phase. The in-beam Mössbauer results [10] show a singlet with a negative isomer shift attributed to the substitutional site and another singlet with positive isomer shift (0.78 mm s^{-1}) attributed to the interstitial site in Ge. However, the isomer shift of the singlet in the present experiment is very small (0.20 mm s^{-1}) compared to 0.78 mm s^{-1} and hence one can rule out the occupation of Fe atoms in the interstitial sites of Ge. In an earlier Mössbauer work on an immiscible system like Fe/Ag [11], it was reported that a singlet with a small positive isomer shift can arise due to Fe atoms in small clusters. In this system isolated Fe atoms give rise to a singlet with an isomer shift of 0.51 mm s^{-1} and bcc like Fe clusters give

rise to a singlet with an isomer shift of 0.04 mm s^{-1}. There is no such work reported for Fe in Ge. However, it is expected to follow a similar trend as in Fe/Ag, because, at low concentration of Fe, the Fe–Ge system is also immiscible. Hence the observation of a singlet with a small positive isomer shift is attributed to clusters of Fe.

Low frequency Raman scattering (LFRS) measurements were carried out in the 60 keV Fe^+ ion-implanted Ge samples to estimate the average size of the Fe clusters. Confined acoustic phonons in metal or semiconductor nanocluster surfaces give rise to low frequency (in the range of a few cm^{-1} to a few tens of cm^{-1}) modes in the vibrational spectrum. The LFRS from a nanocrystal is due to the elastic vibration of the nanocrystal itself. Confined surface acoustic phonons give rise to low frequency modes, which correspond to spheroidal and torsional modes of vibration of a spherical or an ellipsoidal particle. Spherical motions are associated with dilation and they strongly depend on the cluster material through v_l and v_t, where v_l and v_t are the longitudinal and transverse sound velocities, respectively. These modes are characterized by two indices l and n, where l is the angular momentum quantum number and n is the branch number. Here $n = 0$ represents the surface modes. It has been shown that the spheroidal modes with $l = 0, 2$ are Raman active [12, 13]. A surface quadrupolar mode ($l = 2$) appears both in the polarized and depolarized geometry whereas a surface symmetrical mode ($l = 0$) appears only in the polarized geometry. These modes appear at low frequencies in the range of 5–70 cm^{-1} and are generally known as low frequency Raman modes.

Raman peak frequencies of the spheroidal modes [12] with $n = 0$ can be expressed as

$$\omega_s^0 = \frac{0.82 v_l}{dc} \tag{1}$$

$$\omega_s^2 = \frac{0.84 v_t}{dc} \tag{2}$$

where ω_s^0 and ω_s^2 are those of the spheroidal modes with $l = 0$ and 2, respectively, and v_l and v_t are the longitudinal and transverse sound velocities. The sound velocities in Fe are $v_l = 6058$ m s^{-1} and $v_t = 3406$ m s^{-1}. In equations (1) and (2), d is the particle diameter and c is the velocity of light in a vacuum. As the frequency is inversely proportional to the size of the particles, very small sized particles would result in a LFRS peak at a relatively higher wavenumber. They would be too weak in intensity to be detected. Large sized particles would give rise to LFRS peaks at very low wavenumbers, which would merge with the Rayleigh peak. Hence it is possible to detect LFRS peaks lying in the range of 5–40 cm^{-1}, which corresponds to clusters of a few nanometres in size.

Figure 2 shows the LFRS of the 60 keV Fe-implanted Ge samples with various ion fluences. The assignment of angular momentum to the observed modes was done by measuring the LFRS in VV and VH geometry (here the letter V stands for vertical polarization and H for horizontal polarization). In the configurations VV and VH, the first letter represents the mode of polarization of the incident wave while the second letter represents that of the scattered wave. LFRS measurement was carried out in VV and VH geometry in the sample implanted up to a fluence of 5×10^{15} ions cm^{-2} and the plot is given in figure 3. In VH geometry, the reduction in intensity is due to a change in polarization between incident and scattered light. The mode at 39.5 cm^{-1} appeared in both VV and VH geometry and hence it was assigned to $l = 2$ whereas the other mode at 34.0 cm^{-1} appeared only in VH geometry and was assigned to $l = 0$. The LFRS peaks shown in figure 3 were fitted with a Lorentzian function to find the peak position of the LFRS modes. The sizes of the Fe clusters were estimated using equations (1) and (2) and tabulated in table 1. Figure 4 shows the LFRS of the Fe^+ ion-implanted Ge[111] up to a fluence of 2×10^{17} ions cm^{-2} and further irradiated with 1 MeV Ge^+ ions to a fluence of 2×10^{17} ions cm^{-2} at 250 °C. The estimated sizes of Fe clusters are given in table 1.

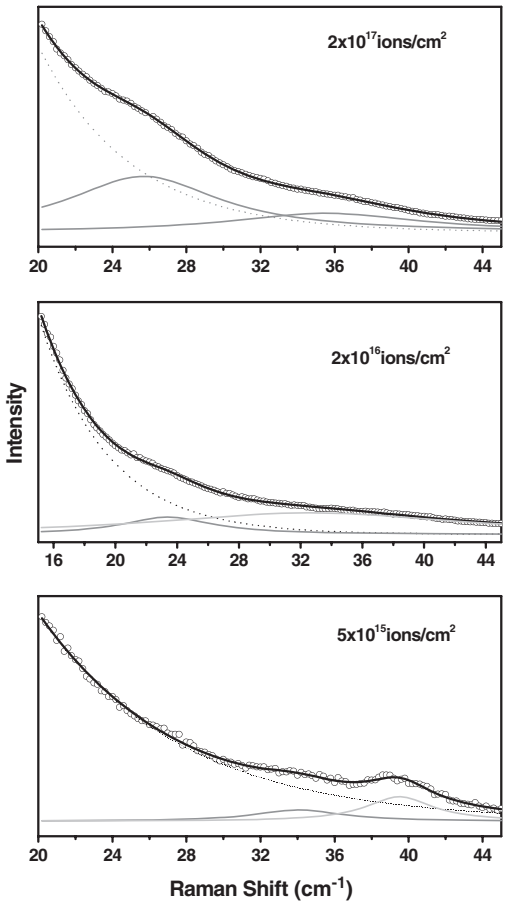

Figure 2. Low frequency Raman scattering of the 60 keV Fe^+ ion-implanted Ge[111] with various fluences. The spectra were fitted with exponential background (dotted line) and Lorentzian peaks (solid line).

Table 1. Parameters as deduced from the fit of the LFRS spectra to the Lorentzian distribution function.

	$l = 0$			$l = 2$		
Fluence (ions cm^{-2})	Raman peak frequency (cm^{-1})	FWHM (cm^{-1})	Fe cluster diameter (nm)	Raman peak frequency (cm^{-1})	FWHM (cm^{-1})	Fe cluster diameter (nm)
5×10^{15}	34.0(5)	5.8(7)	4.86(3)	39.5(1)	4.4(6)	2.41(3)
2×10^{16}	23.3(9)	7.1(3)	7.07(8)	32.6(1)	23.7(7)	2.92(4)
2×10^{17}	25.6(9)	9.9(5)	6.44(6)	35.5(5)	12.5(6)	2.68(2)
Self-ion irradiated	33.4(1)	6.0(9)	4.95(6)	38.6(3)	7.0(0)	2.46(8)

Figure 5 shows the GIXRD pattern of the unimplanted, the Fe^+-implanted Ge and self-ion irradiated samples. The GIXRD pattern of the unimplanted Ge shows the (111) peak. The Fe-implanted Ge samples show broad XRD peaks, which indicate the amorphous nature of Ge. As a function of irradiation fluence, the Ge peaks are broadened, mainly due to defects produced during ion irradiation. The inset of figure 5 shows the GIXRD pattern of the unimplanted and

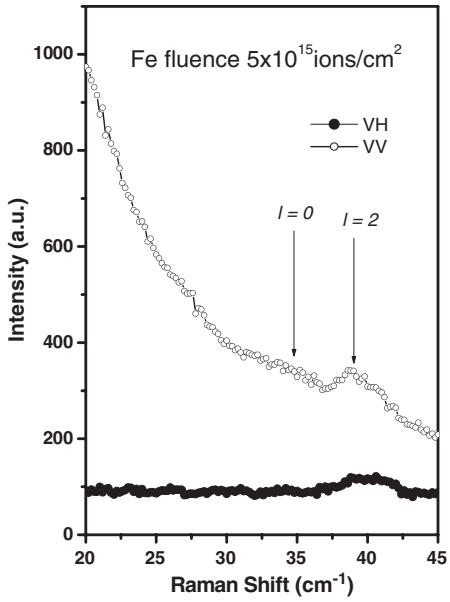

Figure 3. The low frequency Raman scattering of Ge[111] implanted with Fe ions up to a fluence of 5×10^{15} ions cm^{-2}.

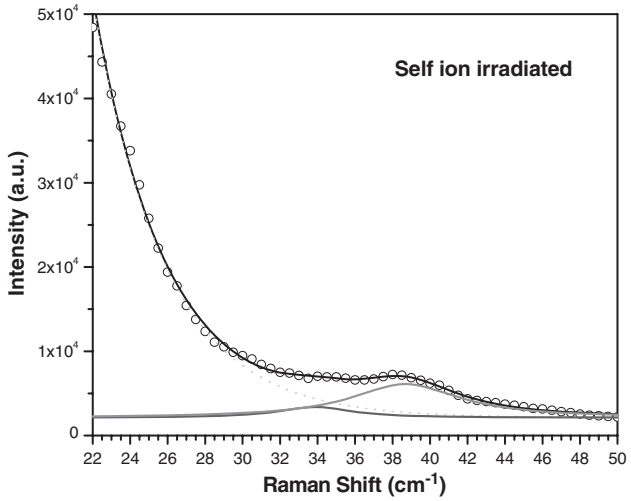

Figure 4. The low frequency Raman scattering of the Fe^+ ion-implanted Ge [111] up to a fluence of 2×10^{17} ions cm^{-2} and further irradiated with 1 MeV Ge^+ ions to a fluence of 2×10^{17} ions cm^{-2} at 250 °C. The spectrum was fitted with exponential background (dotted line) and Lorentzian peaks (solid line).

Fe^+-implanted Ge to fluences of 2×10^{17} ions cm^{-2} and the self-ion irradiated sample in the 2θ range of 40°–60°. One can see the signature of Fe around 44.7° which corresponds to the (110) plane of Fe. Since the Fe has a very low concentration (<10 at.%), the Fe signal is very weak. This result also supports the LFRS and CEMS measurements which show the presence of Fe nanoclusters in the sample implanted to a fluence of 2×10^{17} ions cm^{-2}. This self-ion

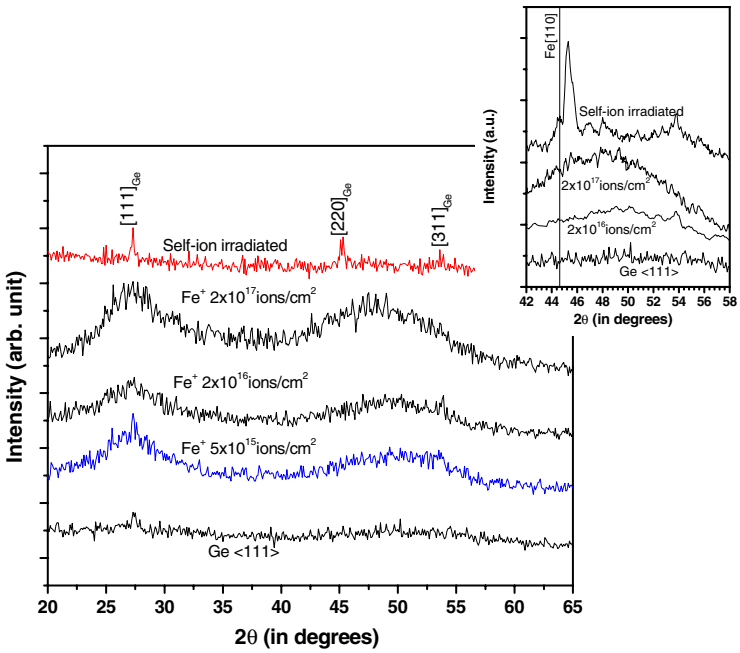

Figure 5. The GIXRD of the 60 keV Fe^+ ion-implanted Ge[111] to various fluences. The inset shows the GIXRD of the unimplanted and the 60 keV Fe^+ ion-implanted Ge[111] to fluences of 2×10^{16} ions cm^{-2} and 2×10^{17} ions cm^{-2} and also the self-ion irradiated sample in the 2θ range 40°–60°.

(This figure is in colour only in the electronic version)

irradiated sample shows the polycrystalline nature in which many Ge peaks can be clearly seen (inset of figure 5). The Fe (110) peak is also seen in the inset of figure 5.

Figure 6 shows the Raman spectra recorded for the unimplanted and the Fe^+ ion-implanted Ge[111]. The Raman spectrum of the unimplanted Ge sample shows the optical phonon mode. The peak position of the optical phonon mode is 299.2($\pm$0.18) cm^{-1} which is characteristic of c-Ge [14]. However, for the sample implanted with Fe ions of fluence of 5×10^{15} ions cm^{-2}, the optical phonon peak disappears as the sample becomes amorphous. With further higher fluences, the transverse optical like (TO-like) phonon mode evolves and the FWHM of this TO-like phonon mode increases with the fluence [15]. The frequency and FWHM of the TO-like phonon is characteristic of amorphous Ge. In amorphous Ge, the TO-like phonon band originates from the phonon density of states (DOS) at the high symmetry points at the edge of the Brillouin zone of its crystalline counterpart. Since the disorder-induced changes in bond angle distribution will modify the phonon DOS, in the first approximation the width of the TO-like phonon should be proportional to the width of the bond angle distribution [15]. The TO-like phonon mode was earlier observed by Cerdeira *et al* [16], and they also reported the stress dependence of optical phonons in c-Si and c-Ge for the orientations [100] and [111], respectively. They were able to determine the parameters $\left[\frac{p+2q}{6\omega_0^2}\right]$, $\left[\frac{p-q}{2\omega_0^2}\right]$ and $\left[\frac{r}{\omega_0^2}\right]$ which describe the strain dependence of the spring constant of these phonons. These authors also related these quantities to the microscopic changes in bond lengths and bond angles of Ge and Si. It is possible to make the connection between bond angle variations ($\Delta\phi$) and the related changes in phonon frequencies. For a distribution of $\Delta\phi$, there will be a related distribution of

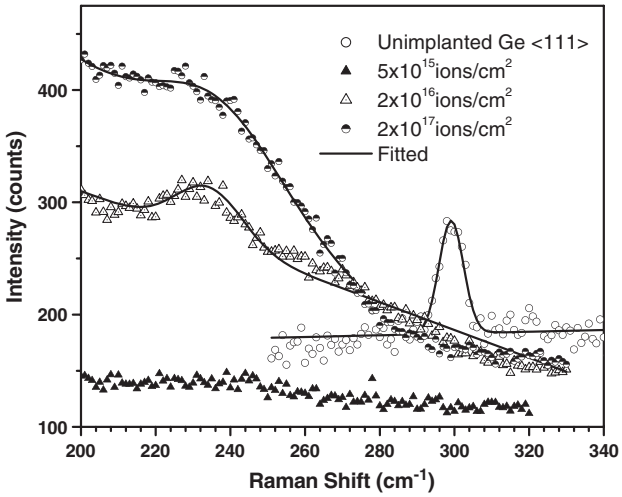

Figure 6. The Raman spectra for the unimplanted Ge[111] and the 60 keV Fe^+ ion-implanted Ge[111] with various fluences.

frequency shift $\Delta\omega$, resulting in a linewidth increase of $\Gamma_\theta = 2\Delta\omega$. The relation between the average bond angle variation $\overline{\Delta\phi}$ and the strain ε is then given by

$$\overline{\Delta\phi} = \tfrac{1}{6}\sum \Delta\phi_{ij} = 2\sqrt{2\varepsilon} \qquad \text{for [111].} \tag{3}$$

Therefore, the relative shift in phonon frequency $\Delta\omega/\omega_0$ caused by $\overline{\Delta\phi}$ may be written as

$$\frac{\Delta\omega}{\omega_0} = \frac{1}{\sqrt{14}}\left[6\left(\frac{p-q}{2\omega_0^2}\right)^2 + 4\left(\frac{r}{\omega_0^2}\right)^2\right]^{\frac{1}{2}}\overline{\Delta\phi} \tag{4}$$

where ω_0 (=250 cm^{-1}) is the unperturbed frequency for a-Ge. Since there is a finite intrinsic linewidth Γ_0 for the crystalline phonon DOS, the total linewidth should be given by

$$\Gamma^2 = \Gamma_0^2 + \Gamma_\theta^2 = \Gamma_0^2 + 4(\Delta\omega)^2 \tag{5}$$

in which Γ_θ is the linewidth due to bond angle deviation. For a-Ge, the intrinsic line width (Γ_0) is 18 cm^{-1}.

In the Fe^+ ion-implanted samples, the TO-like phonon mode is observed at 234.54($\pm$0.69) and 237.51($\pm$0.55) cm^{-1} for fluences of 2×10^{16} ions cm^{-2} and 2×10^{17} ions cm^{-2}, respectively. The FWHM of the TO-like phonon is 43.7 and 68.0 cm^{-1} for fluences of 2×10^{16} ions cm^{-2} and 2×10^{17} ions cm^{-2}, respectively and the corresponding bond angle distortion is estimated to be 7.6° and 12.3° by using equation (5). This is consistent with earlier work in which the bond disorder was observed to increase linearly with the irradiation fluence [17].

The Raman spectrum of the self-ion irradiated sample shows both optical phonon and TO-like phonon modes (figure 7). The presence of an optical phonon mode at 298.47($\pm$0.15) cm^{-1} shows the partial crystallization of a-Ge. A TO-like phonon is observed at 255.89($\pm$1.20) cm^{-1} with a FWHM 54.6 cm^{-1}. Using equation (5) the corresponding bond angle distortion is calculated to be 9.8° and hence the TO-like phonon relaxes by 2.5°. This is consistent with earlier work [17].

Figure 8(a) shows the AFM topograph in 2D view of the unimplanted Ge[111]. It clearly shows that the surface is smooth and featureless. Figure 8(b) shows the AFM topograph in

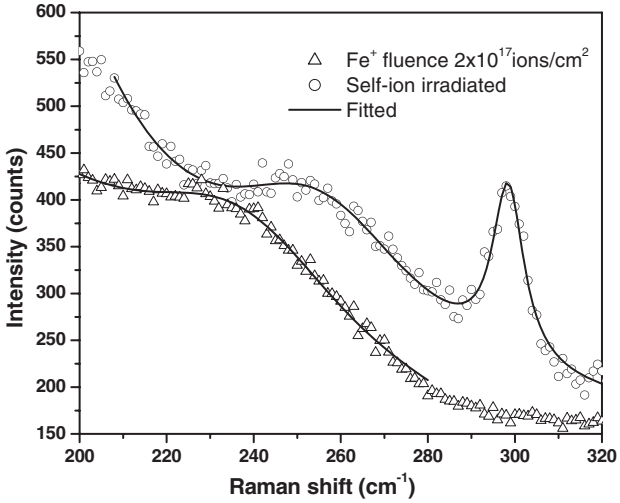

Figure 7. The Raman spectra for the 60 keV Fe^+ ion-implanted Ge[111] with a fluence of 2×10^{17} ions cm^{-2} followed by self-ion irradiation with 1 MeV ions of fluence 3×10^{16} ions cm^{-2} at 250 °C.

2D view of the Fe^+ ion-implanted Ge[111] to a fluence of 2×10^{17} ions cm^{-2}. It shows the presence of a porous layer with a pore diameter of 400 nm and depth around 100 nm. Also, one can see grains with a diameter of ∼200 nm below the porous layer. It has been reported that ion implantation into Ge at room temperature creates severe surface cratering extending several thousand angstroms into the surface, leading to a porous surface structure [18]. During ion irradiation, stochastic removal of atoms or sputtering tends to roughen the surface while the transport driven by surface energy minimization tends to smooth the surface. The observation of a porous layer in the Fe^+-implanted Ge is due to the competition between roughening and smoothing mechanisms; here in particular the sputtering is dominant over the surface smoothing process. However, in the self-ion irradiated sample, the absence of a porous layer is due to the thermal process being dominant over sputtering. The observation of a porous layer is consistent with earlier reports [19]. Figure 8(c) shows the AFM topograph in 2D view of the Ge[111] sample first implanted with Fe^+ ions of fluence 2×10^{17} ions cm^{-2} and then followed by self-ion irradiation with 1 MeV ions of fluence 3×10^{16} ions cm^{-2} at 250 °C. It clearly shows the absence of a porous layer and a grain size of 400 nm. The observation of amorphization along with the formation of a porous layer upon self-ion irradiation on Ge with a fluence of 3×10^{16} ions cm^{-2} at room temperature is reported by Stritzker *et al* [19]. These authors have concluded that the irradiation at higher temperatures (>200 °C) produced neither an amorphous layer nor a porous layer. The present observation of a porous layer is consistent with earlier reports [19].

Before discussing the mechanism of Fe cluster formation, the observations related to Fe nanoclusters will be described briefly. The 60 keV Fe^+ ion implantation in Ge[111] at room temperature produced Fe nanoparticles (3–6 nm) embedded in an amorphous Ge matrix. The *a*-Ge is recrystallized by ion beam annealing the sample at 250 °C with 1 MeV Ge^+ ions. The recrystallized sample contained Fe nanoparticles having a size of 2–4 nm. By CEMS, LFRS and GIXRD measurements, the presence of Fe clusters was observed and their sizes were estimated.

Venugopal *et al* [5, 6] implanted multiple energy Fe ions into Ge using a metal vapour vaccum arc (MEVVA) ion source, which simultaneously produced Fe^+ (25%), Fe^{2+} (68%)

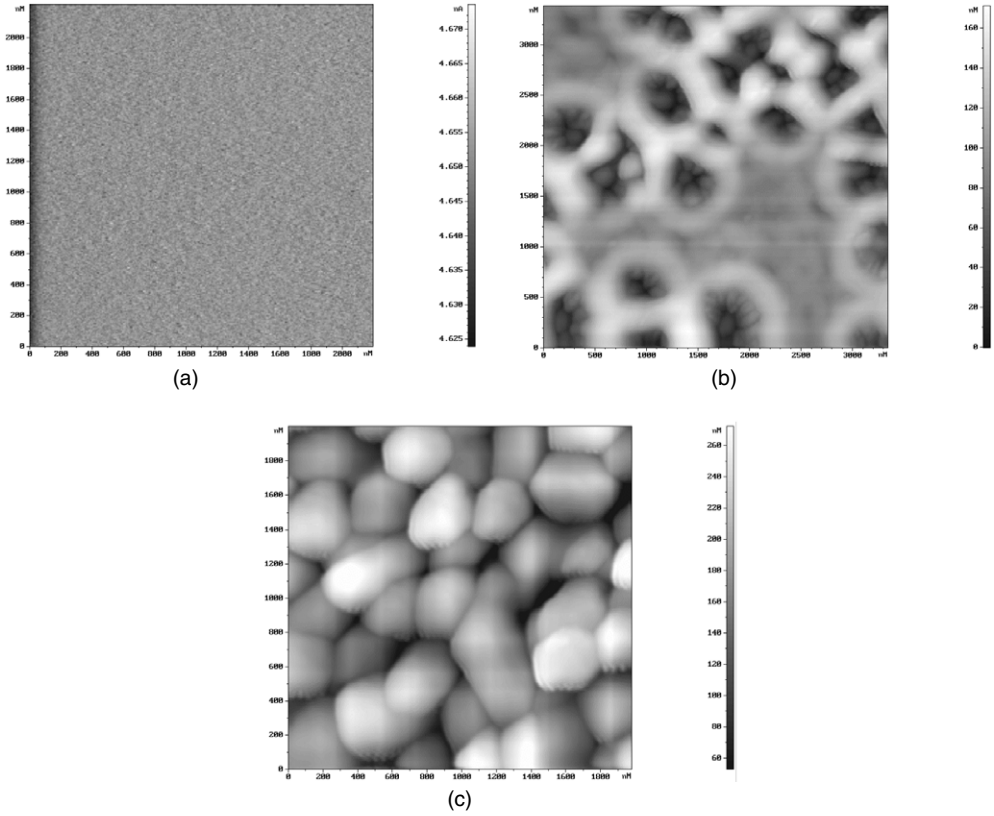

Figure 8. The AFM image of (a) the unimplanted Ge[111], (b) 60 keV Fe^{+} ion-implanted Ge[111] with a fluence of 2×10^{17} ions cm^{-2} and (c) followed by self-ion irradiation with 1 MeV ions of fluence 3×10^{16} ions cm^{-2} at 250 °C.

and Fe^{3+} (7%) with a high current density (54 μA cm^{-2}). They observed a nanosized Fe_3Ge phase at a dose of 2×10^{16} ions cm^{-2} and Fe clusters at a dose of 2×10^{17} ions cm^{-2}. Since the sample was not cooled, the Ge temperature during implantation was 210 °C and the substrate was crystallized due to self-annealing during implantation. Because of this, the authors attributed the formation of Fe clusters to two factors: (i) increase in Fe concentration at high dose which favours clustering of Fe atoms due to low solubility of Fe atoms in Ge and (ii) increase in substrate temperature which enhances reordering of displaced Ge atoms and give rise to clustering of Fe atoms. However, in the present experiments, Fe clusters are produced in the implanted sample itself in which the Ge substrate temperature was always less than 50 °C during implantation, and hence the role of Ge substrate temperature is ruled out in the clustering of Fe atoms. Since the heat of mixing of the Fe–Ge system is positive [1] (when the Fe concentration is <25 at.%), solubility of Fe in Ge is low and hence the chemical driving force assisted the formation of Fe clusters. According to the empirical formula proposed by Rossi *et al* [20], a linear dependence exists between the critical temperature (T_c) for the onset of radiation enhanced diffusion and the average cohesive energy (ΔH_{coh}). Using this empirical relation $T_c = 95.2\Delta H_{coh}$ (eV/atom), we obtain a value of $T_c = 187$ °C for the Fe–Ge system. Since the temperature of irradiation is 50 °C, radiation enhanced diffusion is completely suppressed. Hence Fe clusters are expected to form directly in the collision cascade

where, within the small molten volume along the path of the ions, demixing takes place due to the low solubility of Fe in Ge.

4. Summary

The implantation of 60 keV Fe^+ ions in Ge[111] at room temperature produced Fe nanoparticles (3–6 nm) embedded in amorphous Ge matrix as evident from CEMS, LFRS and GIXRD measurements. The a-Ge is recrystallized by beam annealing of the sample at 250 °C with 1 MeV Ge^+ ions. The recrystallized sample contains Fe nanoparticles having a size of 2–4 nm. In the present experiments, Fe clusters are formed in the implanted sample itself in which the Ge substrate temperature was less than 50 °C during implantation. We rule out any role of Ge substrate temperature during implantation in the clustering of Fe atoms. Since radiation enhanced diffusion is completely suppressed at the temperature of irradiation, the Fe nanoclusters form directly during the irradiation process itself as thermal or radiation enhanced diffusivity is absent.

Acknowledgments

We thank Dr K G M Nair for fruitful discussions. We also thank Dr T K Chini and Dr D Dutta for their help during ion irradiation at the Saha Institute of Nuclear Physics, Kolkatta. We thank Dr M Kamruddin for AFM measurements. The financial support from UGC-DAE CSR, Indore Centre and partial financial support from UGC under SAP III to the Department of Nuclear Physics, University of Madras are gratefully acknowledged.

References

[1] de Boer F R, Boom R, Mattens W C, Midema A R and Niessen A K 1998 *Cohesion in Metals* (Amsterdam: North-Holland)
[2] Ma P, Anderson G W and Norton P R 1999 *Surf. Sci.* **420** 134
[3] Ma P and Norton P R 1997 *Phys. Rev.* B **56** 9881
[4] Regan M J and Bienenstock A 1995 *Phys. Rev.* B **51** 12170
[5] Venugopal R, Sundaravel B, Cheung W Y, Wilson I H, Wang F W and Zhang X X 2001 *Phys. Rev.* B **65** 14418
[6] Venugopal R, Sundaravel B, Wilson I H, Wang F W and Zhang X X 2002 *J. Appl. Phys.* **91** 1410
[7] Brand R A 1987 *Nucl. Instrum. Methods* B **28** 398
[8] Patankar J, Bhandarkar Y V, Kanetkar S M, Ogale S B and Bhide V G 1985 *Nucl. Instrum. Methods* B **7/8** 720
Tomiyoshi S, Yamamoto H and Watanabe H 1966 *J. Phys. Soc. Japan* **21** 709
[9] Sawicki J A and Sawicka B D 1977 *Phys. Status Solidi* **80** K41
[10] Kübler J, Kumm A E, Overhof H, Schwalabach P and Sielemann R 1993 *Z. Phys.* B **92** 155
[11] Morales M A, Passamani E C and Baggio-Saitovitch E 2002 *Phys. Rev.* B **66** 144422
[12] Duval E 1992 *Phys. Rev.* B **46** 5795
[13] Duval E, Boukenter A and Champagnon B 1986 *Phys. Rev. Lett.* **56** 2052
[14] Anderson A (ed) 1973 *The Raman Effect* vol 2 (New York: Dekker)
[15] Desnica-Frankovic I D 2004 *Nucl. Instrum. Methods* B **216** 318
[16] Cerdeira F, Buchanauer C J, Pollak F H and Cardona M 1972 *Phys. Rev.* B **5** 580
Tsu R, Gonzalez-Hernandez J and Pollak F H 1985 *Solid State Commun.* **54** 447
[17] Glover C J, Ridgway M C, Yu K M, Foran G J, Desnica-Frankovic D, Clerc C, Hansen J L and Nylandsted-Larsen A 2001 *Phys. Rev.* B **63** 73204
[18] Appleton B R, Holland O W, Narayan J, Schow O E III, Williams J S, Short K T and Lawson E 1982 *Appl. Phys. Lett.* **41** 711
[19] Stritzker B, Elliman R G and Zou J 2001 *Nucl. Instrum. Methods* B **175–177** 193
[20] Rossi F, Natasi M, Cohen M, Olsen C, Tesmer J R and Egen C 1991 *J. Mater. Res.* **6** 1175